coatings

MDPI

Article

Dual-Function Hybrid Coatings Based on Polytetrafluoroethylene and Cu_2O for Anti-Biocorrosion and Anti-Wear Applications

Guohui Li [1,2], Huan Li [2], Yongkun Xu [3], Ren He [3], Ga Zhang [2,3,4,*] and Zongzhu Liu [1,*]

[1] School of Life Sciences, Qingdao Agricultural University, Qingdao 266109, China; 17852428806@163.com
[2] State Key Laboratory of Solid Lubrication, Lanzhou Institute of Chemical Physics, Chinese Academy of Sciences, Lanzhou 730000, China; lih@licp.cas.cn
[3] Key Laboratory of Science and Technology on Wear and Protection of Materials, Lanzhou Institute of Chemical Physics, Chinese Academy of Sciences, Lanzhou 730000, China; xyk@licp.cas.cn (Y.X.); heren@licp.cas.cn (R.H.)
[4] Qingdao Center of Resource Chemistry & New Materials, Qingdao 266071, China
* Correspondence: gzhang@licp.cas.cn (G.Z.); liuzongzhu@126.com (Z.L.)

Abstract: Corrosion and wear issues of motion components exposed to water-based corrosion mediums, e.g., naval vessels and oil extraction equipment, pose challenges for the lifespan and reliability of the motion systems. In this work, epoxy-based coatings modified with polytetrafluoroethylene (PTFE) and cuprous oxide (Cu_2O) nanoparticles were prepared. The anti-corrosion performance of the coatings was comparatively investigated by electrical impedance spectroscopy and Tafel tests in sterile and sulphate-reducing bacteria (SRB) mediums. Moreover, the tribological behaviors of the coatings were examined under water lubrication conditions. Our results demonstrate that the epoxy coatings lower significantly the corrosion current density i_{corr} and the charge transfer resistance of the electrical double layer R_{ct} of the carbon steel substrate. Interestingly, the hybrid coatings filled with both PTFE and Cu_2O exhibit excellent anti-corrosion and anti-wear performance. After being immersed in the SRB medium for 18 days, the i_{corr} of the pure EP coating and hybrid coatings are 1.10×10^{-7} A_{mp}/cm^2 and 0.3×10^{-7} A_{mp}/cm^2, and the R_{ct} values are 1.04×10^3 $\Omega \cdot cm^2$ and 3.87×10^3 $\Omega \cdot cm^2$, respectively. A solid tribofilm forms on the stainless steel counterface sliding against the hybrid coating, which is surmised to be essential for the low friction coefficients and wear. The present work paves a route for formulating the dual-function coatings of anti-biocorrosion and anti-wear.

Keywords: sulphate-reducing bacteria; biocorrosion; wear; anti-wear

Citation: Li, G.; Li, H.; Xu, Y.; He, R.; Zhang, G.; Liu, Z. Dual-Function Hybrid Coatings Based on Polytetrafluoroethylene and Cu_2O for Anti-Biocorrosion and Anti-Wear Applications. *Coatings* **2024**, *14*, 592. https://doi.org/10.3390/coatings14050592

Academic Editor: Ioana Demetrescu

Received: 11 April 2024
Revised: 26 April 2024
Accepted: 1 May 2024
Published: 9 May 2024

1. Introduction

Corrosion and wear are important factors causing issues such as equipment failures and security risks, etc. [1]. The metallic motion components of naval vessels [2], oil borehole equipment, [3] and wastewater pollution equipment [4] are exposed to seawater, sewage or oilfield produced fluids. In these mediums, a variety of corrosive microorganisms thrive, including sulfate-reducing bacteria, iron bacteria, methanogens, acid-producing bacteria and so on [5–8]. In particular, the motion components lubricated with water often operate in mixed and even boundary lubrication regimes [9]. The tribo-corrosion of the metallic components is a significant challenge regarding the lifespan and reliability of the equipment [10,11]. That is, corrosion caused by aggressive chemicals and microorganisms in the water medium can accelerate the wear of the motion components, and vice versa [12,13].

Microbiologically influenced corrosion (MIC) causes significant financial loss, i.e., approximately 20% of the total corrosion cost of metals globally [14]. Nowadays, to prevent and control MIC, numerous chemical biocides, e.g., glutaraldehyde, 2,2-dibromo-3-nitrilopropionamide and tetrakis hydroxymethyl phosphonium sulfate, are used to

eliminate microorganisms in sewage and oilfield produced fluids [15,16]. However, such chemical biocides usually result in various environmental issues and induce the resistance of bacteria to chemical biocides [17]. Hence, stringent regulations have been established by governments worldwide for controlling the utilization of these chemical biocides. It has been recognized that sulfate-reducing bacteria (SRB) are one of the most common microorganisms inducing MIC [14]. Extracellular polymeric substances (EPS) secreted by SRB attach to the surfaces of metallic materials and form biofilms in which other corrosion products are distributed [18]. The biofilms provide an anaerobic circumstance which is more favorable for the growth and activities of SRB and can aggravate long-term localized corrosion [19].

Several models have been proposed to explain mechanisms governing MIC. SRB can utilize sulfates (SO_4^{2-}) as an electron acceptor and release sulfide ions (S^{2-}) or hydrogen sulfide (H_2S) in the process of metabolism [20]. The S^{2-} produced by SRB can react with Fe^{2+} released from the steel to form FeS, which can cause the blockage of oil pipelines and the degradation of oil quality [21,22]. Moreover, the presence of FeS in the biofilms can promote electron transfer from Fe to SRB [23]. H_2S as corrosive gas itself can cause corrosion and the souring of petroleum reservoirs [22,24]. According to Kuhr's cathode depolarization theory [25,26], SRB can cause the cathodic depolarization and corrosion of steel, and thereby aggravate hydrogen evolution corrosion. Another mechanism of SRB corrosion is known as the theory of extracellular electron transfer (EET) [27,28]. In the absence of a carbon source, SRB may form conductive nanowires and connect with the steel through conductive proteins on their outer membrane to capture electrons from Fe atoms [27,29].

Polymer composites have been recognized as effective anticorrosive coating materials, demonstrating good barrier properties against electrochemical corrosion caused by chemicals in the ocean and chemistry industries [30]. Polymer resins such as epoxy and acrylate are commonly utilized as binder materials of the composite coatings [31–33]. Various formulating strategies and approaches of anti-corrosion composite coatings have been developed and applied successfully. In the last decade, various metallic oxide nanoparticles, e.g., titanium dioxide [34], copper oxide [35] and cerium dioxide [36], and nanosheets, e.g., graphene and its derivatives [37], nano-graphitic carbon nitride [38] and nano-hexagonal boron nitride [39], are dispersed into polymer matrices and their effects on polymers' anti-corrosion performance have been investigated. It has been demonstrated that the addition of the nanofillers is an effective approach for greatly improving the anti-corrosion performance of the polymer coatings. The anti-corrosion mechanisms of nanofillers are ascribed to their complex inhibition effects, which are associated with physical barriers [40], passivation [41], cathodic protection [42] and so on.

However, polymer coatings are susceptible to corrosion caused by biofouling due to the adhesion and growth of bacteria and marine organisms [43]. The anti-corrosion performance of polymer coatings exposed to bacteria mediums have been explored in recent years. The results of Zhu et al. [44] demonstrated that polydimethylsiloxane (PDMS)/cuprous oxide (Cu_2O) composite coating exhibits remarkable antifouling and anti-corrosion resistance against *Pseudomonas aeruginosa, Staphylococcus aureus*, algae and mussels. The authors surmised that Cu irons progressively released from the composite coating can inhibit biofilm formation and bacteria proliferation, whilst the low surface energy of PDMS is less conducive for fouling microorganisms to establish attachment. Zhao et al. [45] reported that core–shell-structured Cu_2O/polyaniline (PANI) dispersed in acrylate coatings showed anti-fouling and anti-corrosion dual-functions. The authors claimed that the possible electrostatic adsorption of the PANI shell to Gram-negative *E. coli* can shorten the function routes of Cu^{2+} for killing the microorganisms. It should be noted that investigations on effects of SRB on the corrosion behaviors of polymer coatings have been rarely reported.

Polymer composites are being increasingly used as tribo-materials subjected to water lubrication conditions thanks to their chemical stability and self-lubrication characteristics. Owing to the low viscosity of water, the water film exhibits a low load-bearing ability. This

is true, especially for sliding at high loads and low speeds [46]. Previous works [47,48] demonstrate that the growth of a solid-lubricating tribofilm at the water-lubricated interface can compensate for the lubrication insufficiency of the water film, and thus greatly improve the tribological performance of the sliding pair.

Epoxy resins have been widely utilized for developing enormous kinds of engineering and functional coatings. Polytetrafluoroethylene (PTFE) is a high-performance polymer demonstrating excellent chemical stability, self-lubrication and superior hydrophobic nature owing to its low surface energy [49]. Cu_2O is an excellent antifouling component in coatings and is more environmentally friendly than conventional fungicides [50]. In this study, epoxy coatings filled with PTFE or/and Cu_2O nanoparticles were prepared and deposited onto a carbon steel substrate. The comparative electrochemical performances of the carbon steel and the epoxy coatings when exposed to sterile and SRB mediums were studied. In order to shed light on hindering corrosion mechanisms, the topographies as well as chemical components of the corroded surfaces were comprehensively analyzed. The tribological behaviors of the epoxy-based coatings were investigated under water lubrication conditions. The aims of this work are to explore a route for formulating dual-function coatings, i.e., anti-corrosion and anti-wear, for applications on metallic components exposed to SRB medium and to elucidate the structure/performance relationship of the epoxy composite coatings.

2. Materials and Methods

2.1. SRB Cultivation

Wastewater originating from produced fluids in the Zhidan oilfield (Shanxi province, Zhidan, China) was cultured using Postgate's medium (Qingdao Haibo Co., Ltd., Qingdao, China) containing (per 1 L of dH_2O): 7.0 g NaCl, 1.2 g $MgCl_2{\cdot}6H_2O$, 0.05 g KH_2PO_4, 1.0 g NH_4Cl, 4.5 g Na_2SO_4, 0.04 g $MgSO_4{\cdot}7H_2O$, 1 mL sodium lactate (60%), 0.1 g yeast extract and 0.03 g sodium citrate placed in a constant temperature incubator with an oxygen-free environment at 30 °C. Prior to culturing the wastewater, Postgate's medium was adjusted to pH 7.0 and sterilized in an autoclave at 121 °C for 30 min. After 7 days culturing, the Postgate's medium turned black, suggesting that the bacterial consortium in the medium is dominated by SRB [51]. The bacterial consortium dominated by SRB was inoculated into Postgate's medium with 2% agar powder at 40 °C. After incubating for 7 days, a pure SRB colony was obtained.

2.2. Materials and Electrode Preparation

Q20 carbon steel (GB/T711-2017 [52], Dongguan LingXing Co., Ltd., Dongguan, China), containing (in wt.%) of 0.07 C, 1.82 Mn, 0.19 Si, 0.17 Ni, 0.01 Mo, 0.023 S, 0.026 Cr, 0.007 P, 0.02 Cu, 0.002 V, 0.028 Al, 0.056 Nb, 0.004 N and 0.0001 B (the rest being Fe), were used for preparing the working electrode. Sections of Q20 carbon steel with dimensions of $10 \times 10 \times 3$ mm^3 were connected with copper wire and sealed in epoxy resin to ensure an exposed work area of 1 cm^2. Then, the work area was polished in succession with 400, 600, and 1000 grit silicon carbide papers.

PTFE powder (Hangzhou Bolong, Co., Ltd., Hangzhou, China) with an average grain diameter of 5 μm and Cu_2O particles (Zhejiang Jiuli, Co., Ltd., Hangzhou, China) with an average size of 50 nm were used as fillers for epoxy-based composite coatings. Figure 1 illustrates the SEM graph of the PTFE powders and the TEM graph of the Cu_2O nanoparticles. To prepare the composite coatings, the fillers, i.e., PTFE, Cu_2O or PTFE/Cu_2O combination, were dispersed into bisphenol A epoxy resin (E51, Nanjing Xingchen Co., Ltd., Nanjing, China) using a vacuum dissolver. Subsequently, the mixture was milled with a three-roll mill. Then, a polyamide curing agent (650, Zhenjiang Danbao Co., Ltd., Zhenjiang, China) was added into the milled resin. Epoxy coatings of approximately 30 μm were sprayed onto the carbon steel and cured at 80 °C for 6 h. Four coatings, referenced as EP (neat epoxy resin), EP/1.5Cu_2O (epoxy resin filled with 1.5 vol.% Cu_2O), EP/15PTFE (epoxy resin filled with 15 vol.% PTFE) and EP/15PTFE/1.5Cu_2O (epoxy resin filled with 1.5 vol.% Cu_2O and 15 vol.% PTFE) were studied and compared directly with carbon steel.

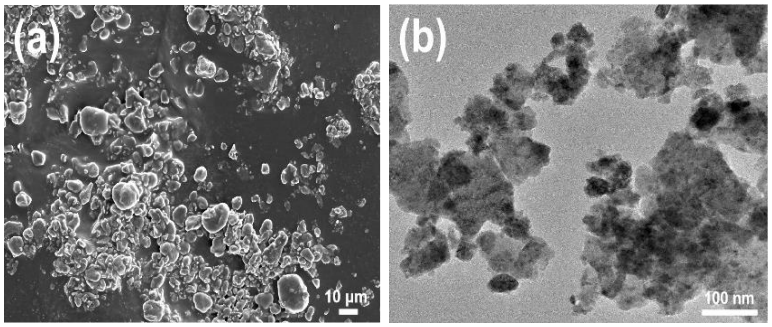

Figure 1. (**a**) SEM graph of PTFE powder and (**b**) TEM graph of Cu_2O nanoparticles.

2.3. Electrochemical Experiments

Electrochemical measurements consisting of electrical impedance spectroscopy (EIS) and potentiodynamic polarization curves were conducted in a three-electrode electrochemical cell with a 0.1 mol/L KCl using electrochemical workstation (CHI660E, Chenhua, Shanghai, Co., Ltd., China). In a three-electrode system, the Q20 carbon steel or epoxy-based coating, with only a 1 cm^2 work area exposed; a saturated calomel electrode (Huayu, Shanghai Co., Ltd., Shanghai, China); and platinum (Huayu, Shanghai Co., Ltd., Shanghai, China) were used as the working electrode, reference electrode and counter electrode, respectively.

Before electrochemical measurement, open-circuit potential (OCP) was monitored for approximately 60 min until it reached a stable value. On the basis of OCP, the EIS was measured under the excitation of a sinusoidal wave with an amplitude of 5 mV and within a frequency range of 10^{-2} to 10^6 Hz. The potentiodynamic polarization curves were measured with a potential scanning range from 250 mV to +300 mV vs. OCP from the cathodic to the anodic direction at a potential scan rate of 0.167 mV min^{-1}.

Before corrosion experiments, the working electrode was sterilized by exposure to ultraviolet light for half a minute. The sterilized work electrode was immersed into sterilized Postgate's medium and inoculated with SRB for 18 days and then removed at the 4th, 11th, and 18th days for electrochemical measurement or corroded surface morphology and components analysis. Before corrosion morphology and components analysis, the removed working electrode was cleaned by using petroleum ether and ultrasonic 30 s and then immersed in 2.5 wt.% glutaraldehyde at 4 °C for 8 h to fix the morphology of SRB, followed by dehydration using a graded aqueous-ethanol series (25 wt.%, 50 wt.%, 75 wt.%, and 100 wt.% for 15 min). A field emission scanning electron microscope (FE-SEM, Merlin Compact, Zeiss, Oberkochen, Germany) equipped with energy-dispersive X-ray spectroscopy (EDS) and X-ray photoelectron spectroscopy (XPS, ESCALAB 250Xi, Thermo Fisher Scientific, Waltham, MA, USA) were used to analyze the morphologies and chemical components of corroded surfaces.

2.4. Tribological Experiments

The tribological characteristics, i.e., friction coefficient and wear rate, of the epoxy-based coatings were measured using a plate-on-ring tribometer (MRH-3, Yihua, Co., Ltd., Jinan, China) at an applied load of 50 N and a sliding velocity of 0.1 m/s over a duration of 2 h. The used ring was made of 304 stainless steel (GB/T 18254-2002 [53], China), with an initial surface roughness (R_a) of 0.12–0.15 μm. Prior to tribo-tests, the steel rings were fully cleaned with petroleum ether.

The wear scar width of the coatings was measured using a digital reading stereoscopic microscope (Olympus BX41, Tokyo, Japan). The specific wear rate (W_s), i.e., wear volume per sliding distance and loading force, was calculated according to the following formula [54].

$$W_s = \frac{L'}{L \cdot F}\left[r^2 \cdot sin^{-1}\left(\frac{W}{2r}\right) - \frac{W}{4}\sqrt{4r^2 - W^2}\right] (mm^3/Nm) \quad (1)$$

where W_s is the specific wear rate ($mm^3/N{\cdot}m$), L' and W are the length and width of the wear scar (mm), r is the radius of steel ring (25 mm), F represents the applied load (N) and L is the total sliding distance (m). And the average value of friction coefficients during the last 10 min of a running-in process was taken as the mean friction coefficient. Each test was conducted a minimum of three times, with mean friction coefficients and specific wear rates calculated for analysis. After the tribo-test, the morphological characterizations and elemental composition mapping of the worn surfaces were analyzed by using SEM and XPS.

3. Results and Discussion

3.1. Electrochemical Measurements

3.1.1. EIS

EIS is efficient for characterizing electrochemical reactions at metal/biofilm interfaces and studying the formation of corrosion products and biofilms [55]. The equivalent circuit model can describe the electrochemical characteristics of an electrochemical system by assuming circuit elements.

Figure 2a–d present the Nyquist plots of the steel and the coatings after being immersed in the sterile medium and SRB mediums. It is well known that a smaller diameter in Nyquist plots suggests a lower corrosion resistance and a higher corrosion rate [56]. As seen from Figure 2a,b, the radius of the arc gradually decreased with increasing immersion time, meaning that the steel was corroded in the medium with or without SRB. Moreover, the arc radius of steel immersed in SRB medium for 18 days is significantly smaller than that of immersed in sterile medium. The steel immersed in SRB medium saw more serious corrosion. As seen from Figure 2c, after immersion in the sterile medium for 18 days, the radius of the arc gradually increased in the following order: EP < EP/1.5Cu_2O < EP/15PTFE < EP/15PTFE/1.5Cu_2O. However, after immersion in the SRB medium for 18 days, the radius of the arc gradually increased in the following order: steel < EP < EP/15PTFE < EP/1.5Cu_2O < EP/15PTFE/1.5Cu_2O.

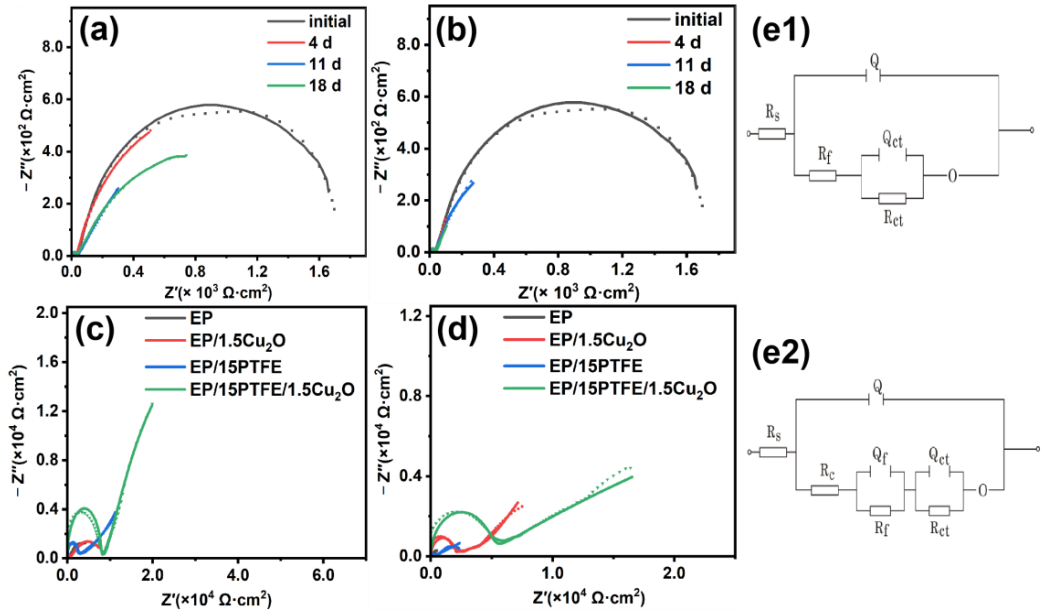

Figure 2. Nyquist plots of Q20 steel after immersion in sterile (**a**) and SRB mediums (**b**); Nyquist plots of coatings after immersion in sterile (**c**) and SRB mediums (**d**); equivalent circuit models for Q20 steel (**e1**) and coatings (**e2**).

Figure 2e1,e2 are the equivalent circuit model for fitting Nyquist plots of Q20 carbon steel and their coatings, respectively. Tables 1 and 2 show the fitting values of Nyquist plots for Q20 steel and the coatings in sterile and SRB medium, respectively. R_s, R_c, R_f and

R_{ct} represent the electrolyte solution resistance, the coating resistance, the resistance the Q20 steel surface layer including the passivation film or the corrosion product film, and the charge transfer resistance of electrical double layer at the carbon steel, respectively. Q_f and Q_{ct} represent surface film capacitance, and electric double-layer capacitance, respectively. O represents the charge transfer free diffusion element. The dotted curve in the Nyquist plots represents the original data obtained from the electrochemical workstation, while the solid curve depicts the fitted data. The trend of the fitted data curve closely matches the original data curve.

Table 1. Fitting data Nyquist plots of Q20 steel in sterile and SRB mediums.

	Corrosion Time (Days)	R_s ($\Omega \cdot cm^2$)	Q_f ($\times 10^{-8}$) ($\mu F \cdot cm^2$)	Q_f-n	R_f ($\times 10$) ($\Omega \cdot cm^2$)	Q_{ct} ($\times 10^{-4}$) ($\mu F \cdot cm^2$)	Q_{ct}-n (10^{-1})	R_{ct} ($\times 10^2$) ($\Omega \cdot cm^2$)	O-Yo (10^{-3})	O-B
Initial	0	6.75	6.78	0.94	2.30	7.25	0.94	7.52	2.90	2.79
Sterile medium	4	5.76	7.25	0.88	2.09	1.69	0.88	7.0	1.87	9.00
	11	5.31	1.69	0.44	2.61	1.78	0.44	5.62	1.15	8.66
	18	5.78	1.78	0.62	2.85	2.89	0.62	4.99	4.00	6.00
SRB medium	4	5.87	3.52	5.48	2.36	7.22	0.77	7.15	6.26	4.22
	11	6.02	2.21	3.15	2.83	1.41	1.00	4.71	2.58	7.73
	18	6.00	1.08	5.27	2.92	2.56	0.89	2.90	1.04	9.92

Table 2. Fitting data Nyquist plots of coatings in sterile and SRB mediums.

	Coatings	R_s ($\times 10^{-2}$) ($\Omega \cdot cm^2$)	Q_f ($\times 10^{-10}$) ($\mu F \cdot cm^2$)	Q_f-n	R_c ($\times 10^2$) ($\Omega \cdot cm^2$)	Q_{ct} ($\times 10^{-5}$) ($\mu F \cdot cm^2$)	Q_{ct}-n (10^{-1})	R_f ($\times 10^3$) ($\Omega \cdot cm^2$)	Q-Yo ($\times 10^{-4}$)	Q-n ($\times 10^{-1}$)	R_{ct} ($\times 10^8$) ($\Omega \cdot cm^2$)	O-Yo ($\times 10^{-1}$)	O-B ($\times 10^{-5}$)
Sterile medium	EP	3.67	1.87	1.00	0.48	3.39	7.61	7.81	3.75	4.64	0.15	9.29	1.39
	EP/1.5Cu_2O	1.01	6.40	1.00	5.24	1.01	2.28	2.38	1.20	2.37	2.11	1.02	1.21
	EP/15PTFE	4.99	6.62	1.00	6.25	1.13	4.09	3.43	1.63	5.20	4.99	5.01	2.28
	EP/15PTFE/1.5Cu_2O	2.40	3.52	1.00	9.21	1.46	3.45	3.55	1.08	8.44	6.29	4.57	3.60
SRB medium	EP	5.60	1.31	1.42	0.66	1.87	1.00	3.87	4.04	6.65	0.01	2.44	8.85
	EP/1.5Cu_2O	9.99	6.91	1.00	6.01	2.14	7.87	4.34	1.42	4.37	2.94	9.82	2.58
	EP/15PTFE	1.89	1.00	1.20	7.04	4.09	8.08	1.05	7.18	1.38	2.28	1.22	1.89
	EP/15PTFE/1.5Cu_2O	2.33	5.35	1.00	9.33	6.95	2.50	1.04	4.19	3.84	5.35	8.45	8.26

R_{ct} in the sterile medium decreases gradually over 4, 11, and 18 days. This behavior is attributed to the corrosion caused by ions in the sterile medium. Previous studies report that the larger the R_{ct}, the lower the charge transfer activity of the metal surface and the less susceptible to corrosion [51]. In the SRB medium, R_{ct} saw no significant change after 4 days of immersion, probably owing to biofilm formation on the steel surface, which can hinder the corrosion of carbon steel. However, after immersion in in the SRB medium for 11 days, the R_{ct} of the steel starts to decrease. Furthermore, the R_{ct} of the steel after being immersed in the SRB medium is lower than that of the steel immersed in the sterile medium for the same number of days. After immersion for 18 days, the R_{ct} of the steel immersed in the SRB medium is lower than that of the steel immersed in the sterile medium by up to 2.09×10^2 $\Omega \cdot cm^2$.

The R_{ct} values of the coatings fitted from the Nyquist plots are summarized in Table 2. After immersion in the sterilized medium, R_{ct} values of the steel and the coatings follow the sequence: steel < EP < EP/1.5Cu_2O < EP/15PTFE < EP/15PTFE/1.5Cu_2O. However, after immersion in the SRB medium, the sequence order of R_{ct} values is as follows: steel < EP < EP/15PTFE < EP/1.5Cu_2O < EP/15PTFE/1.5Cu_2O. When immersed in the sterile medium, EP/15PTFE exhibits higher corrosion resistance than EP/1.5Cu_2O. It is surmised that the hydrophobic feature of PTFE benefits the electrochemical corrosion of the coating [34], whereas Cu_2O nanoparticles are more effective than PTFE particles for enhancing the biocorrosion resistance of the epoxy coating. Interestingly, the above results demonstrate that the Cu_2O nanoparticles and PTFE particles play a synergetic role in enhancing the corrosion resistance of the coatings.

3.1.2. Potentiodynamic Polarization Curves

Figure 3 displays the potentiodynamic polarization curves of the steel after 4, 11, and 18 days of corrosion in the sterile medium and SRB mediums, respectively. Table 3 lists the fitting corrosion current density (i_{corr}) and corrosion potential.

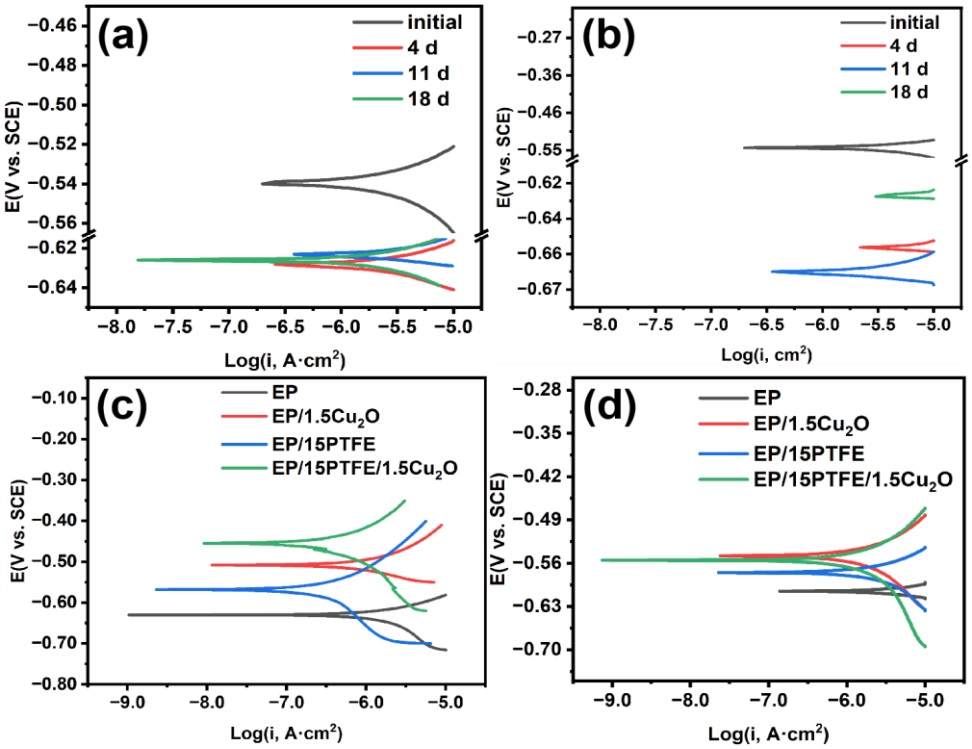

Figure 3. Potentiodynamic polarization curves of the Q20 steel (**a**,**b**) and the coatings (**c**,**d**) after being immersed in sterile (**a**,**c**) and SRB mediums (**b**,**d**) for 18 days.

Table 3. Fitted data from potentiodynamic polarization curves of the Q20 steel immersed in sterile medium.

	Corrosion Time (Days)	Io $\times 10^{-7}$ (A_{mp}/cm^2)	Eo (Volts)	Ba (mv)	Bc (mv)
Initial	0	1.47	−0.54	18.93	−21.63
Sterile medium	4	1.97	−0.62	14.23	−18.18
	11	2.32	−0.65	13.56	−13.56
	18	2.55	−0.62	17.73	−23.32
SRB medium	4	1.32	−0.52	13.56	−13.56
	11	2.95	−0.67	11.14	−7.43
	18	4.17	−0.63	7.80	−7.80

It has been well recognized that the larger the i_{corr}, more susceptible to corrosion [57]. i_{corr} of the steel increases gradually when being immersed in the sterile medium for 4, 11 and 18 days. Nevertheless, after being immersed in the SRB medium for 4 days, i_{corr} decreases, probably due to biofilm formation [58]. The biofilm that forms on the metal surface effectively decreases the ionic and electronic conductivity of steel [59–61]. After immersion for 11 days in the SRB medium, i_{corr} starts to increase. At 18 days immersion in the SRB medium, the i_{corr} of the steel is 1.62×10^{-7} A_{mp}/cm^2 higher than that of the steel immersed for the same period in the sterile medium. These results are consistent with the tendency of aforementioned EIS results. Figure 4 compares the potentiodynamic polarization curves of the steel and the four coatings after 18 days of corrosion in sterilized and SRB mediums.

Table 4 summarizes the i_{corr} fitted from the potentiodynamic polarization curves of the coatings after being immersed in both kinds of mediums. The i_{corr} of the steel and the coatings immersed in the SRB medium follows the sequence: EP > EP/1.5Cu_2O > EP/15PTFE > EP/15PTFE/1.5Cu_2O. The i_{corr} of the steel and the coatings immersed in the sterile medium follows the sequence: EP > EP/15PTFE > EP/1.5Cu_2O > EP/15PTFE/1.5Cu_2O. Note that the i_{corr} results are consistent with the EIS results.

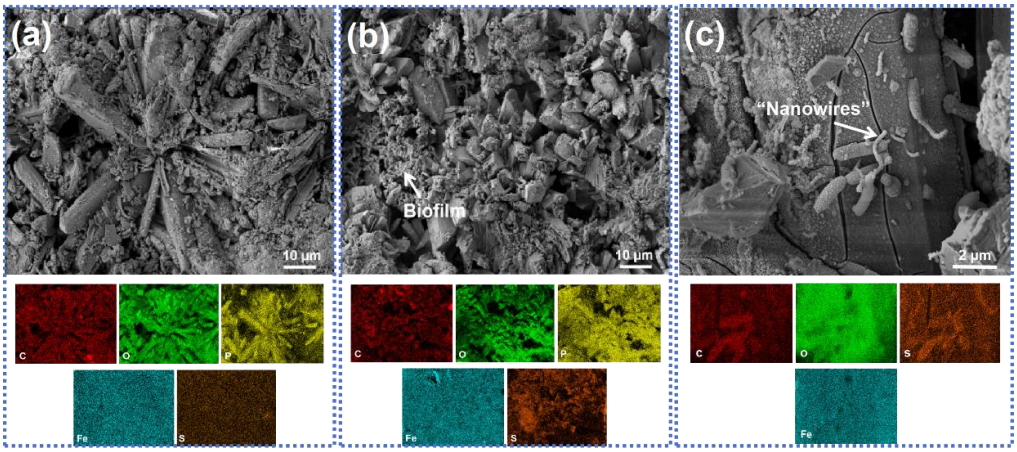

Figure 4. SEM graphs and EDS elemental maps of carbon steel surfaces after being immersed in the sterile medium (**a**) and the SRB medium (**b**,**c**) for 18 days.

Table 4. Fitted data from potentiodynamic polarization curves of the coatings immersed in SRB medium.

	Coatings	Io × 10^{-7} (A_{mp}/cm^2)	Eo (Volts)	Ba (mv)	Bc (mv)
Sterile medium	EP	0.83	−0.62	30.82	−58.45
	EP/1.5Cu_2O	0.62	−0.51	53.57	−45.93
	EP/15PTFE	0.24	−0.46	53.58	−70.48
	EP/15PTFE/1.5Cu_2O	0.20	−0.45	64.32	−86.42
SRB medium	EP	1.10	−0.61	16.90	−14.54
	EP/1.5Cu_2O	0.75	−0.57	40.99	−52.43
	EP/15PTFE	0.35	−0.54	44.45	−79.27
	EP/15PTFE/1.5Cu_2O	0.30	−0.55	72.18	−75.32

3.2. Characterization of Corrosion Morphologies

Figure 4a,b are SEM graphs and EDS elemental maps of Q20 steel after 18 days of corrosion in the sterile and the SRB mediums, respectively. On the corroded surface in the sterile medium, radial rod-like structures containing P and O elements are identified. Consistent with Kadhim Finteel's XRD results of corroded surfaces in a similar medium, the $FePO_4$ is one of the corrosion products [62]. It is surmised that the phosphatization of the steel dominates the corrosion process in this research. On the steel surface immersed in the SRB medium, a gravel-like morphology was generated and a biofilm consisting mainly of S, O and P elements are observed. It has been reported that FeS was generated in the biofilm due to SRB corrosion [51]. The closer inspection of the steel surface shows that "nanowire-like" structures consisting mainly of C, O and S elements are generated in the SRB medium (Figure 4c). Sherar et al. [63] and Gu et al. [27] assumed that such nanowire structures are be conductive and thus aggravate the corrosion of the steel by capturing electrons from the steel substrate.

In order to elucidate the chemical states of the corrosion products on the steel surface, XPS analyses were conducted. Figure 5 shows the XPS spectra of the steel surfaces after immersion 18 days in the sterile medium and the SRB medium. The presence of $FePO_4$ on

the surface immersed in the sterile medium is identified on the P 2p spectrum (Figure 5(a1)), whilst $FePO_4$ and FeO peaks are clearly observed on the Fe 2p spectrum (Figure 5(a2)). These results corroborate that the corrosion products of the steel in the sterile medium are mainly $FePO_4$ and FeO [57]. After 18 days corrosion in the SRB medium, the fingerprints of $FeSO_4$, FeS and FeS_2 are clearly identified on the XPS spectra (Figure 5(b1,b2)). It is thus verified that SRB causes the corrosion of the steel and generates FeS and FeS_2 as corrosion products.

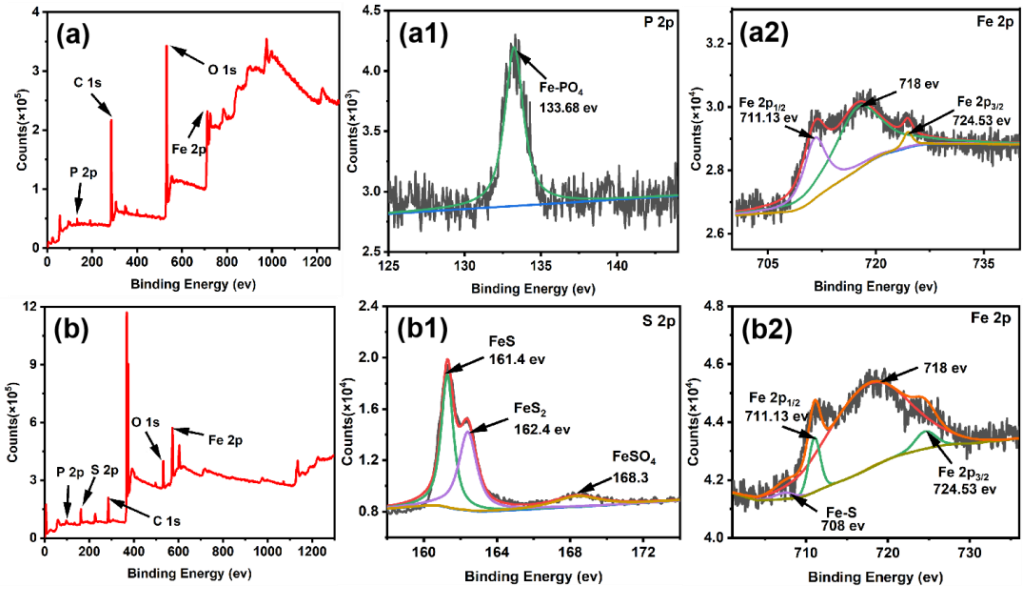

Figure 5. XPS spectra of Q20 steel surfaces after being immersed in the sterile medium (**a**,**a1**,**a2**) and the SRB medium (**b**,**b1**,**b2**) for 18 days.

Figure 6 shows the SEM graphs of EP and EP/15PTFE/1.5Cu_2O coatings after 18 days of corrosion in the sterile and the SRB medium, respectively. Microcracks, as indicated by arrows in Figure 6a, can be seen on the surface of the EP coating. We assume that corrosion by the sterile medium can cause damage to the epoxy chains. After being immersed in the SRB medium, holes were generated on the EP coating, hinting that more severe corrosion occurs in the SRB medium than that in the sterile medium. As consistent with the above results of EIS and potentiodynamic polarization curves, the presence of SRB in the medium aggravates the corrosion damage of the EP coating. No obvious failure marks are noticed on the SEM graphs of the EP/15PTFE/1.5Cu_2O coating immersed for 18 days in both the sterile medium and the SRB medium (c.f. Figure 6c,d). The high corrosion resistance of the hybrid composite coating against SRB corrosion is thus verified. Zhang et al. [64] and Ying et al. [34] reported that the hydrophobicity of PTFE can benefit the corrosion resistance of the coating by decreasing adhesion with SRB. Cu_2O nanoparticles can slow down the permeation of the corrosive medium and release Cu^{2+} to penetrate the cell membrane and destroy the structure of nucleic of the SRB [50,65].

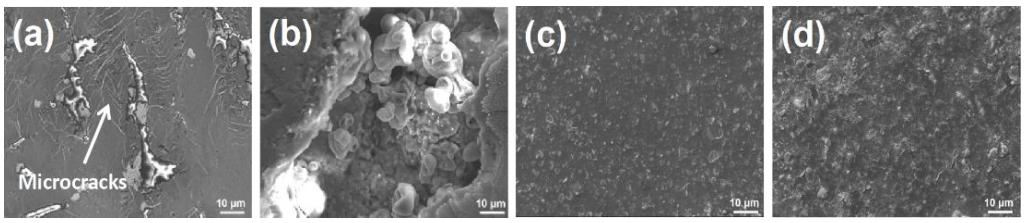

Figure 6. SEM images of EP in (**a**) sterile and (**b**) SRB medium for 18 days; SEM images of EP/1.5Cu_2O/15PTFE in the (**c**) sterile and (**d**) SRB medium for 18 days.

3.3. Tribological Behaviors

Figure 7a compares the friction coefficient evolutions of EP, EP/1.5Cu_2O, EP/15PTFE and EP/1.5Cu_2O/15PTFE coatings obtained from sliding in water at 50 N, 0.1 m/s. The friction coefficient of EP increases quickly and stabilizes at about 0.58. After 40 min of sliding, the test was terminated because of the fast wear of the pure EP coating (the coating was nearly worn off after 40 min). The addition of Cu_2O nanoparticles does not exert a pronounced effect on the friction coefficient evolution. Nevertheless, the addition of Cu_2O nanoparticles significantly improves the wear resistance of the EP coating. Unlike the sliding of EP, EP/1.5Cu_2O was not worn off even after 120 min of sliding. Interestingly, adding 15 vol.% PTFE into EP lowers the friction coefficient from 0.58 to 0.22. Moreover, in comparison to the sliding of pure EP, the friction fluctuation during the sliding of EP/15PTFE is far more suppressed. As elucidated below, the addition of PTFE leads to the formation of a tribofilm, which is deemed essential for improving the boundary lubrication effect of the water-lubricated pair. With respect to the sliding of EP/1.5Cu_2O/15PTFE, a friction evolution tendency similar to the sliding of EP/15PTFE was achieved. It seems that further adding 1.5 vol.% Cu_2O nanoparticles into PTFE-filled epoxy does not affect the friction coefficient.

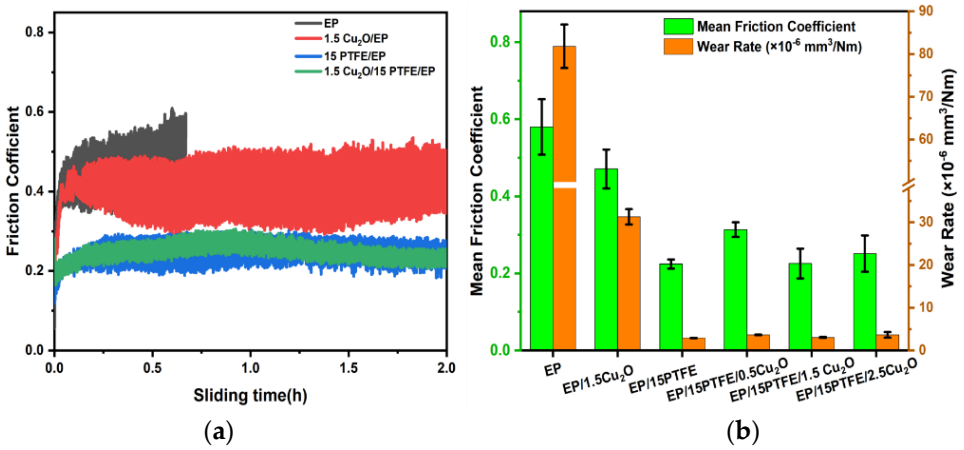

(**a**) (**b**)

Figure 7. (**a**) Evolutions of friction coefficients of EP, EP/1.5Cu_2O, EP/15PTFE and EP/1.5Cu_2O/15PTFE; (**b**) mean friction coefficients and specific wear rates of the coatings investigated.

Figure 7b presents the mean friction coefficient and wear rate of the EP-based coatings investigated. The addition of 15 vol.% PTFE into epoxy resin greatly decreases the wear rate of the coating. That is, in comparison to the wear rate of the EP coating, the wear rate of EP/15PTFE is reduced by up to 96.44%. Further adding Cu_2O nanoparticles at volume fractions from 0.5% to 2.5% into PTFE-filled epoxy does not significantly influence the friction coefficient and wear rate. It is thus demonstrated that the hybrid epoxy-based coatings filled with either PTFE or Cu_2O, i.e., EP/1.5Cu_2O/15PTFE, both exhibit excellent anti-wear and anti-biocorrosion performances.

From the worn surface of the EP coating (Figure 8a), abrasion marks parallel to the sliding direction are observed. Moreover, cracks perpendicular to the sliding direction were generated on the surface. As can be seen in Figure 8b, abrasion furrows are also noticeable on the worn surface of EP/1.5Cu_2O. Nevertheless, unlike the sliding of neat epoxy resin, no crack perpendicular to the sliding direction was generated. The enhancement of wear resistance due to the addition of Cu_2O nanoparticles could be associated with the toughening effect of the nanoparticles [66]. The worn surfaces of EP/15PTFE and EP/1.5Cu_2O/15PTFE are smoother than those of EP and EP/1.5Cu_2O (Figure 8c,d), indicating that the abrasion wear of the coatings containing PTFE is mitigated.

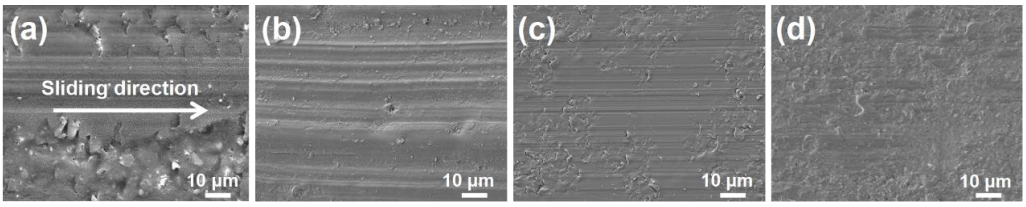

Figure 8. SEM graphs of worn surfaces of EP (**a**), EP/1.5Cu_2O (**b**), EP/15PTFE (**c**) and EP/1.5Cu_2O/15PTFE (**d**) sliding against the steel surface in water lubrication. Arrows indicate the sliding direction.

In order to reveal possible tribochemical actions occurring at the sliding interface of EP/1.5Cu_2O/15PTFE, XPS analyses of the steel counterface were performed. As can be seen in the survey spectrum in Figure 9, C, O, F and Fe elements are identified. The peaks at 284.7 eV, 288.4 eV and 292.4 eV in the C 1s spectrum are assigned to C-C/C=C, C=O and -CF_2-, derived from the tribo-products of epoxy resin and PTFE. The peaks at 688.7 eV in the F 1s spectrum is a signature of -CF_2-, verifying the presence of PTFE tribo-products. Moreover, the new compositions of FeF_2 are detected, corresponding to the peaks at 684.90 eV on the F 1s spectrum and 713.6 eV on the Fe 2p spectrum. Consistent with findings of Ren et al. [67] and Sun et al. [68], the scission of PTFE molecules occurred and oxides and fluorides formed under shear and frictional heat. It is believed that the growth of a solid tribofilm as a result of the complex tribo-chemical actions of PTFE molecules is important as it can compensate for the boundary lubrication insufficiency of the water film.

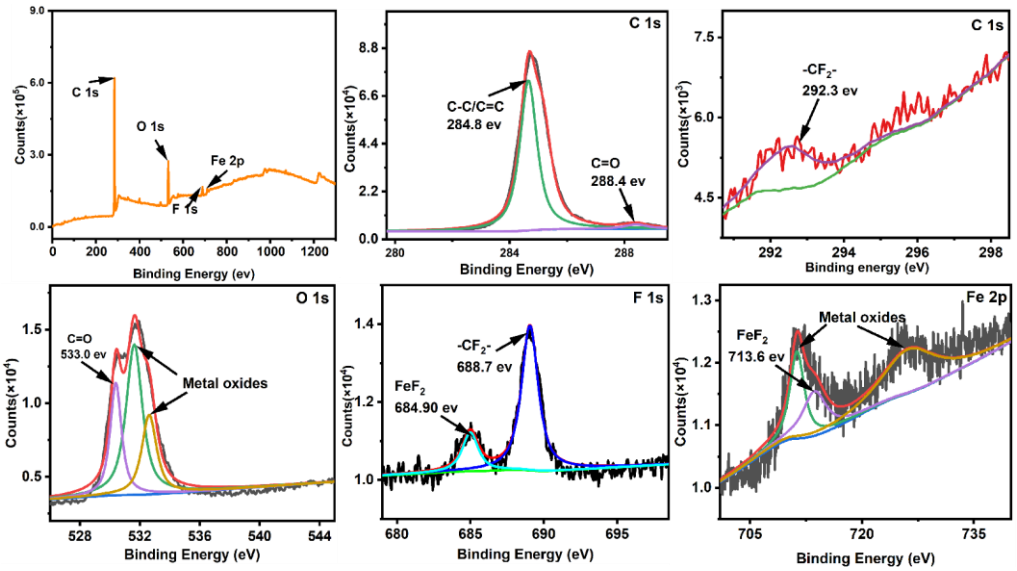

Figure 9. XPS spectra of the steel surface sliding against EP/1.5Cu_2O/15PTFE.

4. Conclusions

In the present work, epoxy-based coatings modified with PTFE and Cu_2O nanoparticles were prepared. The anti-corrosion performance of the coatings was comparatively investigated in sterile and SRB mediums. Moreover, the tribological behaviors of the coatings were examined under water lubrication conditions. Specifically, the corroded and worn surfaces were comprehensively characterized. The following conclusions can be inferred:

(1) The presence of SRB in the medium aggravates the corrosion damage of the carbon steel and coatings. After immersion for 18 days, the R_{ct} of the steel immersed in the SRB medium was lower than that of the steel immersed in the sterile medium by up to 2.09×10^2 Ω·cm^2, and the i_{corr} of the steel was 1.62×10^{-7} A_{mp}/cm^2 higher than that of the steel immersed for the same period in the sterile medium.

(2) The epoxy-based coatings filled with PTFE or/and Cu_2O significantly mitigate the corrosion of the carbon steel. After being immersed in the SRB medium for 18 days, the EP/1.5Cu_2O/15PTFE exhibited the lowest i_{corr} and the highest R_{ct} and no obvious defects and failures were noticed on the corroded surface. The hydrophobic feature of PTFE can benefit the electrochemical corrosion of the coating, whereas Cu_2O nanoparticles are more effective than PTFE particles for enhancing the biocorrosion resistance of the epoxy coating. The synergetic anti-biocorrosion role of PTFE and Cu_2O was identified.

(3) In comparison to neat EP and EP/1.5Cu_2O coatings, the EP-based coatings filled with PTFE exhibit a much improved tribological performance under water lubrication conditions. FeF_2 fluoride and the -CF_2- group are identified on the steel counterface sliding against EP/1.5Cu_2O/15PTFE. It is surmised that tribofilm growth as a result of the tribo-chemical actions of PTFE molecules plays an important role in friction and wear reduction.

(4) The addition of PTFE and Cu_2O significantly improves the anti-corrosion and anti-wear performance of the epoxy resin coating. The present work paves the way for formulating dual-function anti-biocorrosion and anti-wear coatings for motion component applications exposed to water-based corrosion mediums.

Author Contributions: Conceptualization and methodology, G.Z., Z.L., H.L. and G.L.; formal analysis, G.L., Y.X. and R.H.; investigation, G.L., Y.X. and R.H.; resources, G.Z. and Z.L.; data curation, G.L.; writing—original draft preparation, G.L.; writing—review and editing, G.Z. Z.L. and H.L.; supervision, Z.L. and G.Z.; project administration, G.Z. and Z.L.; funding acquisition, G.Z. All authors have read and agreed to the published version of the manuscript.

Funding: The work is supported by the Strategic Priority Research Program of the Chinese Academy of Sciences, grant no. XDB0470201, and International Partnership Program of the Chinese Academy of Science, grant no. 121B62KYSB20210030. The authors gratefully acknowledge the funding from Key R&D Program of Shandong Province, China (grant no. 2023CXPT060).

Institutional Review Board Statement: Not applicable.

Informed Consent Statement: Not applicable.

Data Availability Statement: Data are contained within the article.

Conflicts of Interest: The authors declare no conflicts of interest.

References

1. Hassan, M.H.F.; Mohamed El Amine Ben, S.; Tarek, Z. A comprehensive review of corrosion protection and control techniques for metallic pipelines. *Eng. Fail. Anal.* **2022**, *143*, 106885.
2. Gudze, M.T.; Melchers, R.E. Operational based corrosion analysis in naval ships. *Corros. Sci.* **2008**, *50*, 3296–3367. [CrossRef]
3. Makarenko, V.D.; Makarenko, I.O.; Chernov, V.Y.; Petrovskii, V.A. Corrosion and mechanical resistance in oil borehole equipment. *Chem. Pet. Eng.* **2003**, *39*, 557–562. [CrossRef]
4. Jia, X.; Yuan, S.; Li, B.; Miu, H.; Yuan, J.; Wang, C.; Zhu, Z.; Zhang, Y. Carbon Nanomaterials: Application and prospects of urban and industrial wastewater pollution treatment based on abrasion and corrosion resistance. *Front. Chem.* **2020**, *8*, 600594. [CrossRef]
5. Shi, J.; Wang, S.; Cheng, X.; Chen, S.; Liu, G. Constructing zwitterionic nanofiber film for anti-adhesion of marine corrosive microorganisms. *J. Mater. Sci. Technol.* **2020**, *70*, 145–155. [CrossRef]
6. Vigneron, A.; Alsop, E.B.; Chambers, B.; Lomans, B.P.; Head, I.M.; Tsesmetzis, N. Complementary microorganisms in highly corrosive biofilms from an offshore oil production facility. *Appl. Environ. Microbiol.* **2016**, *80*, 2545–2554. [CrossRef]
7. Sun, Y.-P.; Yang, C.-T.; Yang, C.-G.; Xu, D.-K.; Li, Q.; Yin, L.; Qiu, C.-S.; Liu, D.; Yang, K. Stern–geary constant for X80 pipeline steel in the presence of different corrosive microorganisms. *Acta Metall. Sin. Engl. Lett.* **2019**, *32*, 1483–1489. [CrossRef]
8. Xu, D.; Gu, T.; Lovley, D.R. Microbially mediated metal corrosion. *Nat. Rev. Microbiol.* **2023**, *21*, 705–718. [CrossRef]
9. Zhang, Z.; Ouyang, W.; Liang, X.; Yan, X.; Yuan, C.; Zhou, X.; Guo, Z.; Dong, C.; Liu, Z.; Jin, Y.; et al. Review of the evolution and prevention of friction, wear, and noise for water-lubricated bearings used in ships. *Friction* **2023**, *12*, 1–38. [CrossRef]
10. Roy, M.; Stack, M.M. Tribo-corrosion V 2016—A return to hyderabad. *Tribol. Int.* **2020**, *141*, 105945. [CrossRef]
11. Soltanahmadi, S.; Morina, A.; van Eijk, M.C.P.; Nedelcu, I.; Neville, A. Tribochemical study of micropitting in tribocorrosive lubricated contacts: The influence of water and relative humidity. *Tribol. Int.* **2017**, *107*, 184–198. [CrossRef]

12. Xu, Y.; Qi, H.; Li, G.; Guo, X.; Wan, Y.; Zhang, G. Significance of an in-situ generated boundary film on tribocorrosion behavior of polymer-metal sliding pair. *J. Colloid Interface Sci.* **2018**, *518*, 263–276. [CrossRef]
13. Liu, G.; Zhang, L.; Li, G.; Zhao, F.; Che, Q.; Wang, C.; Zhang, G. Tuning the tribofilm nanostructures of polymer-on-metal joint replacements for simultaneously enhancing anti-wear performance and corrosion resistance. *Acta Biomater.* **2019**, *87*, 285–295. [CrossRef]
14. Anandkumar, B.; George, R.P.; Maruthamuthu, S.; Parvathavarthini, N.; Mudali, U.K. Corrosion characteristics of sulfate-reducing bacteria (SRB) and the role of molecular biology in SRB studies: An overview. *Corros. Rev.* **2016**, *34*, 41–63. [CrossRef]
15. Senthilmurugan, B.; Radhakrishnan, J.S.; Poulsen, M.; Arana, V.H.; Al-Qahtani, M.; Jamsheer, A.F. Microbially induced corrosion in oilfield: Microbial quantification and optimization of biocide application. *J. Chem. Technol. Biotechnol.* **2019**, *22*, 023132. [CrossRef]
16. Piotr, W.; Paweł, Ł.; Elżbieta, S.; Grzegorz, A.; Karol, C.; Szymon, S. Concrete corrosion in a wastewater treatment plant—A comprehensive case study. *Constr. Build. Mater.* **2021**, *303*, 124338.
17. Shi, X.; Zhang, R.; Sand, W.; Mathivanan, K.; Zhang, Y.; Wang, N.; Duan, J.; Hou, B. Comprehensive review on the use of biocides in microbiologically influenced corrosion. *Microorganisms* **2023**, *11*, 2194. [CrossRef] [PubMed]
18. Chan, K.-Y.; Xu, L.-C.; Fang, H.H.P. Anaerobic electrochemical corrosion of mild steel in the presence of extracellular polymeric substances produced by a culture enriched in sulfate-reducing bacteria. *Environ. Sci. Technol.* **2002**, *36*, 1720–1727. [CrossRef]
19. Wang, J.; Yin, S.; Lu, L.; Zhou, J.; Fu, Q. Characterization of microbial-induced concrete corrosion by combining morphology observation and fluorescence staining. *Case Stud. Constr. Mater.* **2022**, *17*, e01586. [CrossRef]
20. Tripathi, A.K.; Thakur, P.; Saxena, P.; Rauniyar, S.; Gopalakrishnan, V.; Singh, R.N.; Gadhamshetty, V.; Gnimpieba, E.Z.; Jasthi, B.K.; Sani, R.K. Gene Sets and Mechanisms of sulfate-reducing bacteria biofilm formation and quorum sensing with impact on corrosion. *Front. Microbiol.* **2021**, *12*, 754140. [CrossRef] [PubMed]
21. Ranlei, Z.; Bo, W.; Dongbo, L.; Yiming, C.; Qiushi, Z. Effect of sulfate-reducing bacteria from salt scale of water flooding pipeline on corrosion behavior of X80 steel. *Eng. Fail. Anal.* **2022**, *142*, 106788.
22. Rajbongshi, A.; Gogoi, S.B. A review on anaerobic microorganisms isolated from oil reservoirs. *World. J. Microbiol. Biotechnol.* **2021**, *37*, 111. [CrossRef] [PubMed]
23. Venzlaff, H.; Enning, D.; Srinivasan, J.; Mayrhofer, K.J.J.; Hassel, A.W.; Widdel, F.; Stratmann, M. Accelerated cathodic reaction in microbial corrosion of iron due to direct electron uptake by sulfate-reducing bacteria. *Corros. Sci.* **2013**, *66*, 88–96. [CrossRef]
24. Gu, T.; Jia, R.; Unsal, T.; Xu, D. Toward a better understanding of microbiologically influenced corrosion caused by sulfate reducing bacteria. *J. Mater. Sci. Technol.* **2018**, *35*, 631–636. [CrossRef]
25. King, R.A.; Miller, J.D.A. Corrosion by the Sulphate-reducing Bacteria. *Nature* **1971**, *233*, 491–492. [CrossRef]
26. Iverson, W.P. Corrosion of iron and formation of iron phosphide by desulfovibrio desulfuricans. *Nature* **1968**, *217*, 1265–1267. [CrossRef]
27. Gu, T.; Wang, D.; Lekbach, Y.; Xu, D. Extracellular electron transfer in microbial biocorrosion. *Curr. Opin. Electrochem.* **2021**, *29*, 100763. [CrossRef]
28. Anguita, J.; Pizarro, G.; Vargas, I.T. Mathematical modelling of microbial corrosion in carbon steel due to early-biofilm formation of sulfate-reducing bacteria via extracellular electron transfer. *Bioelectrochemistry* **2022**, *145*, 108058. [CrossRef] [PubMed]
29. Dou, W.; Liu, J.; Cai, W.; Wang, D.; Jia, R.; Chen, S.; Gu, T. Electrochemical investigation of increased carbon steel corrosion via extracellular electron transfer by a sulfate reducing bacterium under carbon source starvation. *Corros. Sci.* **2019**, *150*, 258–267. [CrossRef]
30. Xu, H.; Zhang, Y. A review on conducting polymers and nanopolymer composite coatings for steel corrosion protection. *Coatings* **2019**, *9*, 807. [CrossRef]
31. Kausar, A. Corrosion prevention prospects of polymeric nanocomposites: A review. *J. Plast. Film Sheeting* **2018**, *35*, 181–202. [CrossRef]
32. Pourhashem, S.; Saba, F.; Duan, J.; Rashidi, A.; Guan, F.; Nezhad, E.G.; Hou, B. Polymer/inorganic nanocomposite coatings with superior corrosion protection performance: A Review. *J. Ind. Eng. Chem.* **2020**, *88*, 29–57. [CrossRef]
33. Kausar, A. Performance of corrosion protective epoxy blend-based nanocomposite coatings: A review. *Polym. Plast. Tech. Mater.* **2019**, *59*, 658–673. [CrossRef]
34. Ying, L.; Wu, Y.; Nie, C.; Wu, C.; Wang, G. Improvement of the tribological properties and corrosion resistance of epoxy–PTFE composite coating by nanoparticle modification. *Coatings* **2020**, *11*, 10. [CrossRef]
35. Zhu, L.; Tang, Y.; Cao, S.; Jiang, J.; Wu, C.; Zhao, K. Enhanced anti-microbial corrosion of nano-CuO-loaded Ni coatings on pipeline steels in simulation environment of natural gas transportation pipeline. *Ceram. Int.* **2023**, *49*, 5543–5549. [CrossRef]
36. Zhang, W.; Wang, H.; Lv, C.; Chen, X.; Zhao, Z.; Qu, Y.; Zhu, Y. Effects of CeO_2 geometry on corrosion resistance of epoxy coatings. *Surf. Eng.* **2019**, *36*, 175–183. [CrossRef]
37. Guo, R.; Li, W.; Wang, X.; Lv, Y.; Chen, M.; Chen, Z.; Liu, Z.; Han, G.-C. Antimicrobial corrosion study of the epoxy coating with the graphene oxide supported Schiff base quaternary ammonium salt additives. *Mater. Today Commun.* **2023**, *35*, 105517. [CrossRef]
38. Yang, G.; Chen, T.; Feng, B.; Weng, J.; Duan, K.; Wang, J.; Lu, X. Improved corrosion resistance and biocompatibility of biodegradable magnesium alloy by coating graphite carbon nitride (g-C3N4). *J. Alloys Compd.* **2019**, *770*, 823–830. [CrossRef]

39. Huang, Z.; Zhao, W.; Zhao, W.; Ci, X.; Li, W. Tribological and anti-corrosion performance of epoxy resin composite coatings reinforced with differently sized cubic boron nitride (CBN) particles. *Friction* **2020**, *9*, 104–118. [CrossRef]
40. Cui, M.; Ren, S.; Qiu, S.; Zhao, H.; Wang, L.; Xue, Q. Non-covalent functionalized multi-wall carbon nanotubes filled epoxy composites: Effect on corrosion protection and tribological performance. *Surf. Coat. Technol.* **2018**, *340*, 74–85. [CrossRef]
41. Wu, Y.; Jiang, F.; Qiang, Y.; Zhao, W. Synthesizing a novel fluorinated reduced graphene oxide-CeO_2 hybrid nanofiller to achieve highly corrosion protection for waterborne epoxy coatings. *Carbon* **2021**, *176*, 39–51. [CrossRef]
42. Ma, Q.; Wang, L.; Sun, W.; Yang, Z.; Wang, S.; Liu, G. Effect of chemical conversion induced by self-corrosion of zinc powders on enhancing corrosion protection performance of zinc-rich coatings. *Corros. Sci.* **2021**, *194*, 109942. [CrossRef]
43. Balagna, C.; Perero, S.; Ferraris, S.; Miola, M.; Fucale, G.; Manfredotti, C.; Battiato, A.; Santella, D.; Vernè, E.; Vittone, E.; et al. Antibacterial coating on polymer for space application. *Mater. Chem. Phys.* **2012**, *135*, 714–722. [CrossRef]
44. Zhu, P.-Y.; Feng, D.-Q.; Yasir, M.; Song, W.-L.; Hafeez, M.A.; Zhang, C.; Liu, L. Enhanced antifouling capability of PDMS/Cu_2O-anchored Fe-based amorphous coatings. *Surf. Coat. Technol.* **2023**, *475*, 130–192. [CrossRef]
45. Zhao, Y.; Tian, S.; Lin, D.; Zhang, Z.; Li, G. Functional anti-corrosive and anti-bacterial surface coatings based on cuprous oxide/polyaniline microcomposites. *Mater. Des.* **2022**, *216*, 110589. [CrossRef]
46. Lancaster, J.K. A review of the influence of environmental humidity and water on friction, lubrication and wear. *Tribol. Int.* **1990**, *23*, 371–389. [CrossRef]
47. Yu, P.; Li, G.; Zhang, L.; Zhao, F.; Guo, Y.; Pei, X.-Q.; Zhang, G. Role of SiC submicron-particles on tribofilm growth at water-lubricated interface of polyurethane/epoxy interpenetrating network (PU/EP IPN) composites and steel. *Tribol. Int.* **2021**, *153*, 106611. [CrossRef]
48. Qi, H.; Hu, C.; Zhang, G.; Yu, J.; Zhang, Y.; He, H. Comparative study of tribological properties of carbon fibers and aramid particles reinforced polyimide composites under dry and sea water lubricated conditions. *Wear* **2019**, *436*, 203001. [CrossRef]
49. Bian, D.; Li, J.; Zhao, Y.; Wang, Y. Investigation of tribological and corrosion properties in ceramic/PTFE coating. *Surf. Eng.* **2022**, *3*, 2–6.
50. Li, H.; Luo, S.; Zhang, L.; Zhao, Z.; Wu, M.; Li, W.; Liu, F.-Q. Water- and acid-Sensitive Cu_2O@Cu-MOF nano sustained-release capsules with superior antifouling behaviors. *ACS Appl. Mater. Interfaces* **2021**, *14*, 1910–1920. [CrossRef]
51. Xie, F.; Wang, Y.; Wang, D.; Sun, D.; Zhou, Y.; Wang, Y. Influence of anion and sulfate-reducing bacteria on the stress corrosion behavior and mechanism of X70 steel in a marine mud environment. *Eng. Fail. Anal.* **2023**, *143*, 106834. [CrossRef]
52. Du, D.; Ye, G.; Pu, Z.; Zhang, W. *High Quality Carbon Structural Steel Hot Rolled Steel Plate and Steel Strip: GB/T 711-2017 Standard*; China Standard Press: Beijing, China, 2017.
53. Shen, J.; Lei, J.; Lua, Y. *High Carbon Chromium Bearing Steel: GB/T 18254– 2002 Standard*; China Standard Press: Beijing, China, 2002.
54. Zhao, F.; Zhang, L.; Li, G.; Guo, Y.; Qi, H.; Zhang, G. Significantly enhancing tribological performance of epoxy by filling with ionic liquid functionalized graphene oxide. *Carbon* **2018**, *136*, 309–319. [CrossRef]
55. Cetin, D.; Aksu, M.L. Corrosion behavior of low-alloy steel in the presence of desulfotomaculum sp. *Corros. Sci.* **2009**, *51*, 1584–1588. [CrossRef]
56. Fan, Y.; Chen, C.; Zhang, Y.; Liu, H.; Liu, H.; Liu, H. Early corrosion behavior of X80 pipeline steel in a simulated soil solution containing Desulfovibrio desulfuricans. *Bioelectrochemistry* **2021**, *141*, 107880. [CrossRef]
57. Wang, G.; Li, H.; Li, P.; Li, X.; Wang, Y. Effect of cerium on the microstructure and anti-corrosion performance of Al-Zn coatings. *Surf. Coat. Technol.* **2023**, *473*, 130046. [CrossRef]
58. Sachie, W.; Saad, A.-S.; Will, P.G.; Christopher, P.; Raman, R.K.S. Sulphate reducing bacteria (SRB) biofilm development and its role in microbial corrosion of carbon steel. *Front. Mater.* **2024**, *11*, 1360869.
59. Yang, Y.; Xiao, C.; Yang, Y.; Liang, B. Research on the reliability of X70 steel gas pipelines under SRB main control factors. *Mater. Corros.* **2022**, *73*, 687–702. [CrossRef]
60. El Saeed, A.M.; Abd El-Fattah, M.; Azzam, A.M.; Dardir, M.M.; Bader, M.M. Synthesis of cuprous oxide epoxy nanocomposite as an environmentally antimicrobial coating. *Int. J. Biol. Macromol.* **2016**, *89*, 190–197. [CrossRef]
61. Wan, H.; Zhang, T.; Wang, J.; Rao, Z.; Zhang, Y.; Li, G.; Gu, T.; Liu, H. Effect of alloying element content on anaerobic microbiologically influenced corrosion sensitivity of stainless steels in enriched artificial seawater. *Bioelectrochemistry* **2023**, *150*, 108367. [CrossRef]
62. Noor, N.M.; Yahaya, N.; Abdullah, A.; Tahir, M.M.; Sing, L.K. Microbiologically influenced corrosion of X-70 carbon steel by desulfovibrio vulgaris. *Adv. Sci. Lett.* **2012**, *13*, 312–316. [CrossRef]
63. Sherar, B.W.A.; Power, I.M.; Keech, P.G.; Mitlin, S.; Southam, G.; Shoesmith, D.W. Characterizing the effect of carbon steel exposure in sulfide containing solutions to microbially induced corrosion. *Corros. Sci.* **2011**, *53*, 955–960. [CrossRef]
64. Zhang, D.; Zhuo, L.; Xiang, Q. Electrophoretic deposition of polytetrafluoroethylene (PTFE) as anti-corrosion coatings. *Mater. Lett.* **2023**, *346*, 134524. [CrossRef]
65. Gurianov, Y.; Nakonechny, F.; Albo, Y.; Nisnevitch, M. Antibacterial composites of cuprous oxide nanoparticles and polyethylene. *Int. J. Mol. Sci.* **2019**, *20*, 439. [CrossRef]
66. Cong, L.; Yefei, L.; Jing, S.; Bo, L.; Yuzhou, D.; Ronn, G.; Yimin, G.; Intizar Ali, S.; Siyong, Z.; Alfred Iing Yoong, T. Interfacial characteristics and wear performances of iron matrix composites reinforced with zirconia-toughened alumina ceramic particles. *Ceram. Int.* **2021**, *48*, 1293–1305.

67. Ren, Y.; Gao, K.; Ying, S.; Zhao, Y.; Zhang, L.; Guo, D.; Xie, G. Significant enhancement of tribological properties of microcapsule/epoxy composites in the presence of high loads by incorporating PTFE. *Wear* **2023**, *204*, 514–515. [CrossRef]
68. Sun, W.; Liu, X.; Liu, K.; Wang, W.; Ye, J. Ultralow wear PTFE composites filled with beryllia and germania particles. *Wear* **2020**, *450–451*, 203270. [CrossRef]